PREDICTION OF UAV POSITIONS USING PARTICLE SWARM OPTIMISATION-BASED KALMAN FILTER

Jian Zhou,* Yu Su,** Yuhe Qiu,** Xiaoyou He,** and Zhihong Rao*

Abstract

The traditional Kalman filter (KF) algorithm solely relies on the historical positioning information of the unmanned aerial vehicle (UAV) itself for UAV position prediction. However, it fails to accurately estimate the position after a longer period of time. To address this issue, this paper proposes an improved PSO-KF algorithm. The algorithm utilises *a priori* route information to generate virtual measurement data and performs real-time state corrections, thereby enhancing the accuracy of position estimation. Additionally, to overcome the challenge of acquiring statistical characteristics of measurement data noise, this paper introduces a particle swarm optimisation algorithm to enhance and optimise the measurement noise covariance matrix. Mathematical simulation results verify that the proposed algorithm outperforms the traditional KF in UAV position prediction, particularly in longer time prediction scenarios, with significant improvements observed.

Key Words

PSO-KF, virtual measurement, prediction.

1. Introduction

An unmanned aerial vehicle (UAV) is an autonomous aircraft that operates without a human pilot. UAVs have various applications, including reconnaissance, surveillance, tactical missions, and more. They are used in disaster scenarios to provide visual surveillance and aid in locating survivors. UAVs are also utilised for aerial imaging of farmland, assessing growing conditions, and gathering topographic data of various terrains. Additionally, drones are employed to collect water samples in the ocean for studying marine life and the chemical properties of seawater and sediment [1]–[6]. Insect-inspired flying robots combine biology and computing, offering efficient flight, resilience, and versatility, thereby opening new possibilities in the field of drones [7]–[9].

Drone position prediction plays a crucial role in UAV operations and applications, enabling operators to effectively control and manage flight paths and destinations. In military and security sectors, drone position prediction technology aids in identifying and predicting the flight paths of enemy drones, facilitating necessary defensive measures. In the commercial sector, it helps optimise drone operations, enhancing operational efficiency and safety. For instance, logistics companies utilise drone location prediction to manage delivery routes, improving cargo transportation efficiency. Moreover, drone position prediction is utilised in weather forecasting, assisting meteorologists in predicting the path and intensity of natural disasters, such as hurricanes, enabling proactive measures [10]–[15].

Regarding UAV position prediction, certain papers [16] and [17] estimate UAV manoeuvre acceleration using a constructed Kalman filter (KF) and LiDAR data, and subsequently solve the integral to obtain the UAV's position in the future. However, this method has limitations in predicting long-term positions and incurs higher costs due to the requirement of LiDAR sensors. Another paper [18] assumes UAV motion follows the Dubins curve, but its applicability is limited. Papers [19]–[21] employ deep learning methods for estimation, which eliminates the need for UAV motion modelling but requires substantial computational resources and may not meet real-time prediction requirements under hardware constraints. Paper [22] utilises a particle swarm algorithm to optimise filter parameters and improve state estimation accuracy, but it only uses sensor history data in constructing the KF, which fails to address sudden acceleration changes during the prediction process.

To address the issue of inaccurate position estimation caused by sudden changes in UAV manoeuvre acceleration during prediction, this paper proposes a novel KF algorithm. The algorithm incorporates *a priori* route information to construct virtual measurement data and

* University of Electronic Science and Technology of China, Chengdu, China; e-mail: zhoujian@cmii.chinamobile.com; 843926543@qq.com

** China Mobile Chengdu Institute of Research and Development, Chengdu, China; e-mail: suyu@cmii.chinamobile.com; qiuyuhe@cmii.chinamobile.com; xiaoyouhe132@gmail.com

Corresponding author: Yu Su

Recommended by Ponnambalam S.G.
(DOI: 10.2316/J.2024.206-1060)

performs real-time state corrections, thereby enhancing position estimation accuracy. Additionally, a particle swarm optimisation algorithm is introduced to overcome the challenge of obtaining statistical characteristics of measurement data noise, further improving prediction accuracy in the proposed KF algorithm mentioned above.

2. UAV Equations of Motion and Observation Equations

Define the navigation coordinate system ($o_F x_F y_F z_F$):

The origin of the navigation coordinate system is the position of the UAV at the moment of takeoff, noted as origin o_F. The $o_F x_F$ is in the local horizontal plane and points due north, while the $o_F y_F$ points due east, and the $o_F z_F$ is determined by the right-hand rule. This coordinate system is solidly connected to the Earth at the moment of UAV takeoff, and the rotation of the Earth is not considered here, so this coordinate system can be considered as an inertial coordinate system [12].

2.1 Equation of Motion

Define the position, velocity, and acceleration of the UAV in the navigation coordinate system as x_r, v_r, and a_r, respectively.

The state variable x of the drone consists of the position, velocity, and acceleration of the drone, namely:

$$x = \begin{bmatrix} x_r^T & v_r^T & a_r^T \end{bmatrix}^T \tag{1}$$

Use the Singer model to describe the acceleration of the drone, namely

$$\dot{a}_{\mathrm{rx}} = -\lambda_x a_{\mathrm{rx}} + w_{\mathrm{tx}} \tag{2}$$
$$\dot{a}_{\mathrm{ry}} = -\lambda_y a_{\mathrm{ry}} + w_{\mathrm{ty}} \tag{3}$$
$$\dot{a}_{\mathrm{rz}} = -\lambda_z a_{\mathrm{rz}} + w_{\mathrm{tz}} \tag{4}$$

Among them, λ_x, λ_y, and λ_z represent the reciprocal of the drone's manoeuvring time constant in the x, y, and z directions. A smaller value of this indicates that the drone tends to perform uniform acceleration motion, while a larger value indicates that the drone tends to perform uniform velocity motion. w_{tx}, w_{ty}, and w_{tz} represent zero-mean Gaussian white noise.

The motion equation is as follows:

$$\begin{cases} \dot{x}_r = v_r \\ \dot{v}_r = a_r \\ \dot{a}_r = -\lambda a_r + w_t \end{cases} \tag{5}$$

Where λ is a diagonal matrix composed of λ_x, λ_y, and λ_z, w_t is a vector matrix composed of w_{tx}, w_{ty}, and w_{tz}. the following equation of state:

$$\dot{x} = F_s x + w_s \tag{6}$$

Among: $F_s = \begin{bmatrix} 0 & 0 & 0 & 1 & 0 & 0 & 0 & 0 & 0 \\ 0 & 0 & 0 & 0 & 1 & 0 & 0 & 0 & 0 \\ 0 & 0 & 0 & 0 & 0 & 1 & 0 & 0 & 0 \\ 0 & 0 & 0 & 0 & 0 & 0 & 1 & 0 & 0 \\ 0 & 0 & 0 & 0 & 0 & 0 & 0 & 1 & 0 \\ 0 & 0 & 0 & 0 & 0 & 0 & 0 & 0 & 1 \\ 0 & 0 & 0 & 0 & 0 & 0 & -\lambda_x & 0 & 0 \\ 0 & 0 & 0 & 0 & 0 & 0 & 0 & -\lambda_y & 0 \\ 0 & 0 & 0 & 0 & 0 & 0 & 0 & 0 & -\lambda_z \end{bmatrix}$

After discretising the above equation with a certain period Δt, we get:

$$\Phi_s = \exp(F_s \Delta t) \tag{7}$$

Then the discretised equation of state is

$$x(k+1) = \Phi_s x(k) + w_s(k) \tag{8}$$

The dynamic noise vector $\omega_s(k)$ is a sequence of Gaussian white random vectors.

$$\omega_s(k) = \begin{bmatrix} 0 & 0 & 0 & 0 & 0 & 0 & w_{\mathrm{tx}} & w_{\mathrm{ty}} & w_{\mathrm{tz}} \end{bmatrix}^T \tag{9}$$

And

$$E[\omega_s(k)] = 0 E[\omega_s(k) {\omega_s}^T(k)] = Q \tag{10}$$

2.2 Observation Equation

Since the UAV contains its own positioning system, its positioning system outputs the UAV status information at each moment, which includes: UAV position and velocity information. Therefore, the observation equation is established as follows:

$$y = Hx + v \tag{11}$$

Among: $H = \begin{bmatrix} 1 & 0 & 0 & 0 & 0 & 0 & 0 & 0 & 0 \\ 0 & 1 & 0 & 0 & 0 & 0 & 0 & 0 & 0 \\ 0 & 0 & 1 & 0 & 0 & 0 & 0 & 0 & 0 \\ 0 & 0 & 0 & 1 & 0 & 0 & 0 & 0 & 0 \\ 0 & 0 & 0 & 0 & 1 & 0 & 0 & 0 & 0 \\ 0 & 0 & 0 & 0 & 0 & 1 & 0 & 0 & 0 \end{bmatrix}$

where v is a column vector consisting of a combination of position and velocity accuracy output from the UAV positioning system.

3. Improved Kalman Filtering Algorithm

3.1 A Priori Observation Information

The route in Fig. 1 consists of two segments of the fold AB and BC, where the coordinates of points A, B, and C are $[x_a, y_a, z_a]$, $[x_b, y_b, z_b]$, and $[x_c, y_c, z_c]$, respectively.

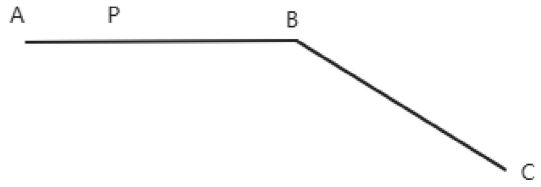

Figure 1. Prior route information.

Point P represents a point on the route, and the coordinates are denoted by $[x_p, y_p, z_p]$. Therefore, the route expressions in Fig. 1 are as follows:

$$\begin{cases} \dfrac{x_p - x_a}{x_b - x_a} = \dfrac{y_p - y_a}{y_b - y_a} = \dfrac{z_p - z_a}{z_b - z_a} & x_a \le x_p \le x_b \\ \dfrac{x_p - x_b}{x_c - x_b} = \dfrac{y_p - y_b}{y_c - y_b} = \dfrac{z_p - z_b}{z_c - z_b} & x_b \le x_p \le x_c \end{cases} \tag{12}$$

The UAV regulatory platform oversees the monitoring of UAVs, which are categorised into cooperative and non-cooperative types. In this context, we will focus solely on cooperative UAVs, which follow pre-planned flight paths. Pre-planned flight paths are typically composed of line segments, as shown in Fig. 1. Assuming that the UAV follows the route in Fig. 1, the point $[x_{\mathrm{rx}}, x_{\mathrm{ry}}, x_{\mathrm{rz}}]$ is the current position of the UAV, the following constraints can be obtained here:

$$\begin{cases} \dfrac{x_{\mathrm{rx}} - x_a}{x_b - x_a} = \dfrac{x_{\mathrm{ry}} - y_a}{y_b - y_a} = \dfrac{x_{\mathrm{rz}} - z_a}{z_b - z_a} & x_a \le x_{\mathrm{rx}} \le x_b \\ \dfrac{x_{\mathrm{rx}} - x_b}{x_c - x_b} = \dfrac{x_{\mathrm{ry}} - y_b}{y_c - y_b} = \dfrac{x_{\mathrm{rz}} - z_b}{z_c - z_b} & x_b \le x_{\mathrm{ry}} \le x_c \end{cases} \tag{13}$$

it can be converted to:

$$\begin{cases} \begin{cases} (x_{\mathrm{rx}} - x_a)(y_b - y_a) - (x_{\mathrm{ry}} - y_a)(x_b - x_a) = 0 \\ (x_{\mathrm{rx}} - x_a)(z_b - z_a) - (x_{\mathrm{rz}} - z_a)(x_b - x_a) = 0 \\ (x_{\mathrm{ry}} - y_a)(z_b - z_a) - (x_{\mathrm{rz}} - z_a)(y_b - y_a) = 0 \end{cases} & P \in [A, B] \\ \begin{cases} (x_{\mathrm{rx}} - x_b)(y_c - y_b) - (x_{\mathrm{ry}} - y_b)(x_c - x_b) = 0 \\ (x_{\mathrm{rx}} - x_b)(z_c - z_b) - (x_{\mathrm{rz}} - z_b)(x_c - x_b) = 0 \\ (x_{\mathrm{ry}} - y_b)(z_c - z_b) - (x_{\mathrm{rz}} - z_b)(y_c - y_b) = 0 \end{cases} & P \in [B, C] \end{cases} \tag{14}$$

Further expressed as:

$$\begin{cases} \begin{cases} x_{\mathrm{rx}}(y_b - y_a) - x_{\mathrm{ry}}(x_b - x_a) = x_a(y_b - y_a) - y_a(x_b - x_a) \\ x_{\mathrm{rx}}(z_b - z_a) - x_{\mathrm{rz}}(x_b - x_a) = x_a(z_b - z_a) - z_a(x_b - x_a) \\ x_{\mathrm{ry}}(z_b - z_a) - x_{\mathrm{rz}}(y_b - y_a) = y_a(z_b - z_a) - z_a(y_b - y_a) \end{cases} & P \in [A, B] \\ \begin{cases} x_{\mathrm{rx}}(y_c - y_b) - x_{\mathrm{ry}}(x_c - x_b) = x_b(y_c - y_b) - y_b(x_c - x_b) \\ x_{\mathrm{rx}}(z_c - z_b) - x_{\mathrm{rz}}(x_c - x_b) = x_b(z_c - z_b) - z_b(x_c - x_b) \\ x_{\mathrm{ry}}(z_c - z_b) - x_{\mathrm{rz}}(y_c - y_b) = y_b(z_c - z_b) - z_b(y_c - y_b) \end{cases} & P \in [B, C] \end{cases} \tag{15}$$

3.2 Improved Filtering Algorithm

In this section, an improved KF algorithm (CKF) is proposed. The course constraint equation of (15) is approached as a virtual sensor, incorporating the subsequent measurement equation:

$$y_c = H_c x + v_c \tag{16}$$

Among:

$$H_c = \begin{cases} \begin{bmatrix} y_b - y_a & x_a - x_b & 0 & 0\ 0\ 0\ 0\ 0\ 0 \\ z_b - z_a & 0 & x_a - x_b & 0\ 0\ 0\ 0\ 0\ 0 \\ 0 & z_b - z_a & y_a - y_b & 0\ 0\ 0\ 0\ 0\ 0 \\ 0 & 0 & 0 & 0\ 0\ 0\ 0\ 0\ 0 \\ 0 & 0 & 0 & 0\ 0\ 0\ 0\ 0\ 0 \\ 0 & 0 & 0 & 0\ 0\ 0\ 0\ 0\ 0 \end{bmatrix} & P \in [A, B] \\ \begin{bmatrix} y_c - y_b & x_b - x_c & 0 & 0\ 0\ 0\ 0\ 0\ 0 \\ z_c - z_b & 0 & x_b - x_c & 0\ 0\ 0\ 0\ 0\ 0 \\ 0 & z_c - z_b & y_b - y_c & 0\ 0\ 0\ 0\ 0\ 0 \\ 0 & 0 & 0 & 0\ 0\ 0\ 0\ 0\ 0 \\ 0 & 0 & 0 & 0\ 0\ 0\ 0\ 0\ 0 \\ 0 & 0 & 0 & 0\ 0\ 0\ 0\ 0\ 0 \end{bmatrix} & P \in [B, C] \end{cases} \tag{17}$$

The measured value of this virtual sensor is then always:

$$y_c = \begin{cases} \begin{bmatrix} x_a(y_b - y_a) - y_a(x_b - x_a) \\ x_a(z_b - z_a) - z_a(x_b - x_a) \\ y_a(z_b - z_a) - z_a(y_b - y_a) \end{bmatrix} & P \in [A, B] \\ \begin{bmatrix} x_b(y_c - y_b) - y_b(x_c - x_b) \\ x_b(z_c - z_b) - z_b(x_c - x_b) \\ y_b(z_c - z_b) - z_b(y_c - y_b) \end{bmatrix} & P \in [B, C] \end{cases} \tag{18}$$

Therefore, when the measurement information is available, the measurement equation is 11. When the measurement information is not updated, *i.e.*, when it is only predicted, the measurement equation is converted from the above constraint, *i.e.*, (16).

The algorithm for the filter is formulated as follows:

$$\widehat{X}(k/k-1) = F_s \widehat{X}(k-1/k-1) \tag{19}$$

$$P(k/k-1) = \Phi_s P(k-1/k-1)\Phi_s^T + Q \tag{20}$$

if(measurement data update)

$$H_j = H \tag{21}$$

else

$$H_j = H_c \tag{22}$$

end

$$S(k) = H_j P(k/k-1) H_j^T + R \tag{23}$$

$$\gamma(k) = Z(k) - H_j \widehat{X}(k/k-1) \tag{24}$$

if($\|S(k)\|_2 \ge \chi * \gamma^T(k)\gamma(k)$)

$$K(k) = P(k/k-1) H_j^T S^{-1}(k) \tag{25}$$

$$\widehat{X}(k/k) = \widehat{X}(k/k-1) + K(k)\gamma(k) \tag{26}$$

$$P(k/k) = [I - K(k)H_j]\, P(k/k-1) \tag{27}$$

else

$$\widehat{X}(k/k) = \widehat{X}(k/k-1) \tag{28}$$

$$P(k/k) = P(k/k-1) \tag{29}$$

end

The above equation $\chi*$ is the protection threshold value of the new interest, which prevents the KF state from being corrected by the wrong measurement information, and this method can improve the robustness of Kalman filtering.

The flowchart of the modified KF is as follows:

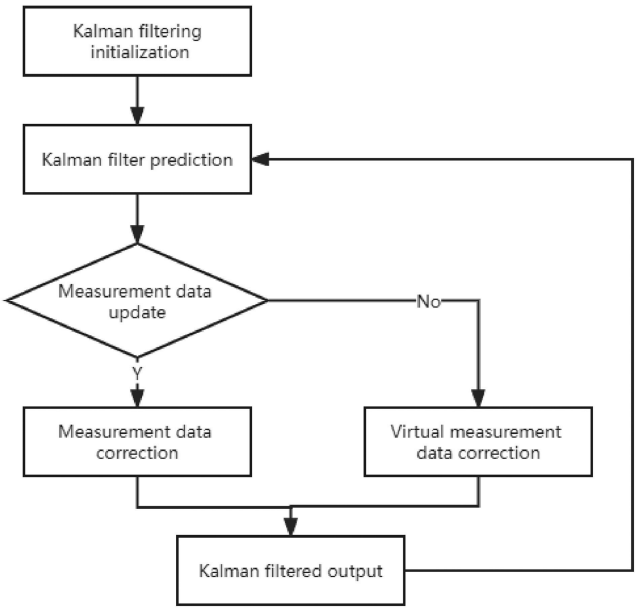

Figure 2. Improved Kalman filtering.

4. Particle Swarm Optimised Improved Kalman Filter

4.1 Introduction to Particle Swarm Optimisation

The particle swarm algorithm is an algorithm for solving an optimal problem by simulating birds searching for food: it assumes that a flock of birds is searching for food randomly in an area where there is only one piece of food, and all birds do not know where the food is, but they know how far their current location is from the food, and then they find the food based on collaboration and information sharing among individuals in the flock.

In the particle swarm optimisation algorithm, each solution can be represented by a bird (particle), and the objective function is the food source that the flock needs to find. The process of finding the optimal solution involves two types of behaviour: individual behaviour and group behaviour.

Individual Behaviour: The particle updates its position according to its own optimal solution in the search process.

Population Behaviour: The particle updates its position according to the optimal solution of the population in the search process.

Suppose N particles form a 1-particle swarm and each particle is a D-dimensional vector, then the position of each particle is:

$$x_i = x_{i1}, x_{i2}, \ldots, x_{\mathrm{iD}} \quad i = 1, 2, \ldots, N \tag{30}$$

The fitness value is calculated by substituting it into the fitness function (the objective function of the optimisation problem), and the position of the optimal fitness value experienced by the ith particle is noted as the individual historical optimum:

$$P_{\mathrm{besti}} = P_{\mathrm{best1}}, P_{\mathrm{best2}}, \ldots, P_{\mathrm{bestD}} \quad i = 1, 2, \ldots, N \tag{31}$$

The optimal position experienced by the entire particle population is noted as the global optimum:

$$G_{\mathrm{besti}} = G_{\mathrm{best1}}, G_{\mathrm{best2}}, \ldots, G_{\mathrm{bestD}} \quad i = 1, 2, \ldots, N \tag{32}$$

After finding these two optimal values above, the particle updates its velocity and position by the following equation.

$$\begin{aligned} V_{i+1} &= V_i + c1 * \mathrm{rand} * (P_{\mathrm{besti}} - x_i) \\ &\quad + c2 * \mathrm{rand} * (G_{\mathrm{besti}} - x_i) \end{aligned} \tag{33}$$

$$x_{i+1} = x_i + V_{i+1} \tag{34}$$

In the above equation, x_i is the current position of the particle. $c1$ and $c2$ are the learning factors. According to the above equation, it is known that each bird will depart in the direction optimal for itself and the population [23].

4.2 Optimisation of Noise Covariance Matrices

The PSO algorithm is used to optimise the noise covariance matrix in the improved KF introduced in the previous section online. Subsequently, employing the methodology outlined in Section 3.2, the filtering estimation is conducted on the present state of the UAV in order to extract the state information at time k denoted as $\widehat{X}_k$.

Substituting $\widehat{X}_k$ into the observation equation $y = Hx$, The resulting observation vector $\widehat{y}_k$ is obtained. The observation residual vector is: $V_k = \widehat{y}_k - y_k$.

Smaller discrepancies between the estimated value and its measurement indicate a more accurate estimation of the UAV's state. As a result, the difference between the estimated and measured values can serve as the fitness function to be minimised, and it can be expressed as follows:

$$R = \arg_R \min \frac{1}{N} \sum_{i=0}^{N} \|V_{k-i}\|_2^2 \tag{35}$$

where $\|\bullet\|_2$ means the Euclidean distance, N is the samples involved in the optimisation of covariance matrices R.

The flowchart of the algorithm is as follows:

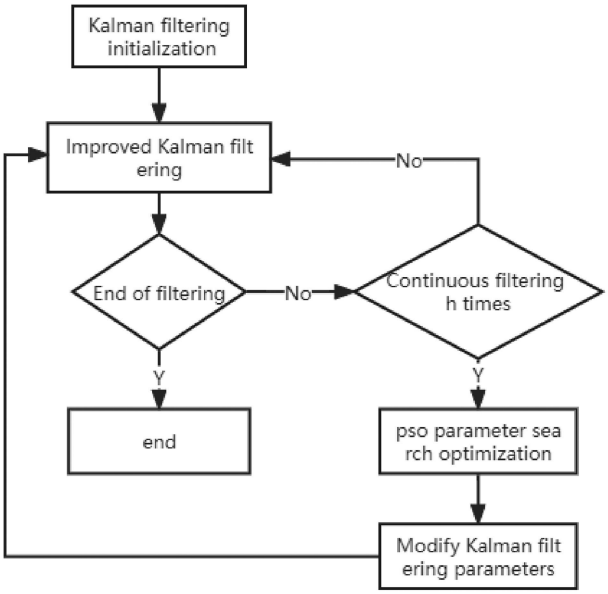

Figure 3. Particle swarm optimisation-based KF.

5. Simulation Experiment and Analysis

With the above analysis, simulation experiments are conducted in this section to verify. The simulation conditions are: the initial position of the UAV in the inertial navigation coordinate system is $[0, 0, -10]$, the initial velocity is $[0, 0, 0]$, and the flight is extended along the route shown in Fig. 4. The acceleration data noise of its UAV is 0.2 m/s^2, the output period is 10 ms, the whole simulation duration is 16 s, and the prediction time is 9 s starting from the 7$^{\text{th}}$ second.

Figure 4 shows the UAV route in horizontal space, which consists of two sections of folded lines, both of which have a height of 10 m and whose turning point coordinates are $[8, 8, -10]$.

To assess the effectiveness of the particle swarm optimisation-based Kalman filtering algorithm (PSO-KF), a comparison was conducted between the proposed method and the approach outlined in [24]. Reference [24] utilises a neural network to estimate the noise covariance of the KF. The simulation comparison results are depicted in Fig. 5.

In Fig. 5, the red solid line represents the real-time estimation error of the traditional KF, the green line indicates the real-time estimation error of the NN+KF approach, and the blue line corresponds to the estimation error of the PSO-KF. Both the PSO-KF and the approach from [24] outperform the KF-based position estimation. This improvement is due to the adjustment of the noise covariance matrix R based on the error between measurements and estimations. The differences in performance between the PSO-KF and [24] approach are relatively minor.

The comprehensive effectiveness of the enhanced Kalman Filtering algorithm (PSO-CKF) is evaluated by contrasting it with the methodologies outlined in [25]

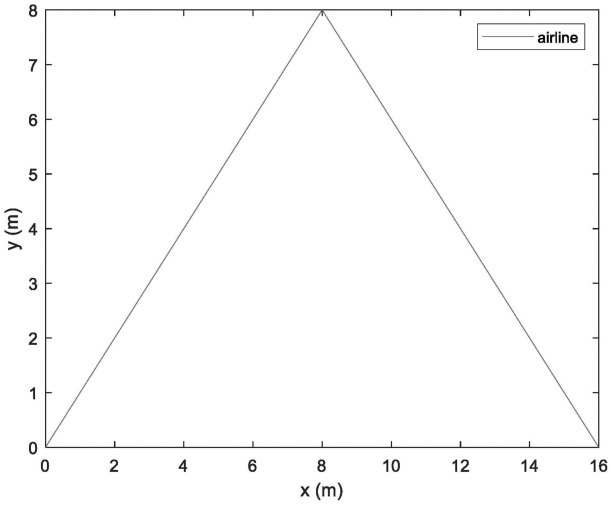

Figure 4. Two-dimensional display of routes.

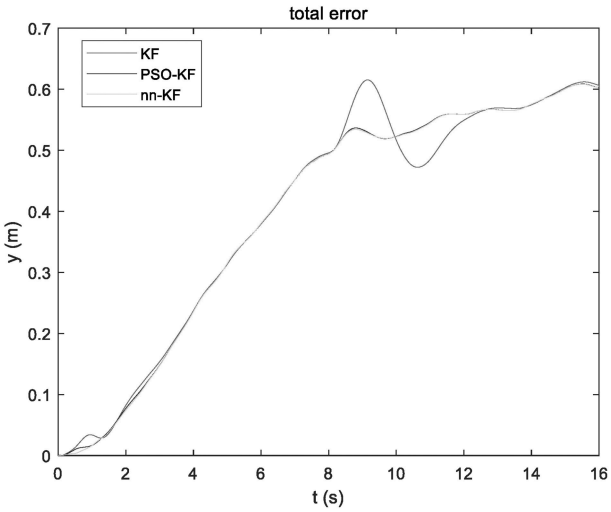

Figure 5. Comparison of different methods.

and [26]. Reference [25] introduces an adaptive unscented Kalman filtering (AUKF) algorithm, which integrates an additional algorithm for real-time adaptation of covariance matrices R and Q. Reference [26] presents a distinct approach utilising random weighting to estimate systematic errors within the observation model (RWKF).

The observations drawn from Fig. 6 emphasise that when encountering a change in direction along the route, the KF, PSO-KF, AUKF, and RWKF all exhibit predictions that follow the existing trajectory. This behaviour leads to notable deviations from the actual path. In contrast, the PSO-CKF demonstrates its unique capability by projecting a trajectory that aligns better with the true path.

Figure 7 depicts the error curves for various filtering algorithms, all of which initiate their predictions from the 7th second and continue for a prediction duration of 9 s.

The statistics presented in Table 1 illustrate the errors between the position predictions and the true values for the five filtering algorithms at intervals of 1 s, 5 s, and 9 s. This indicates that PSO-CKF significantly enhances the

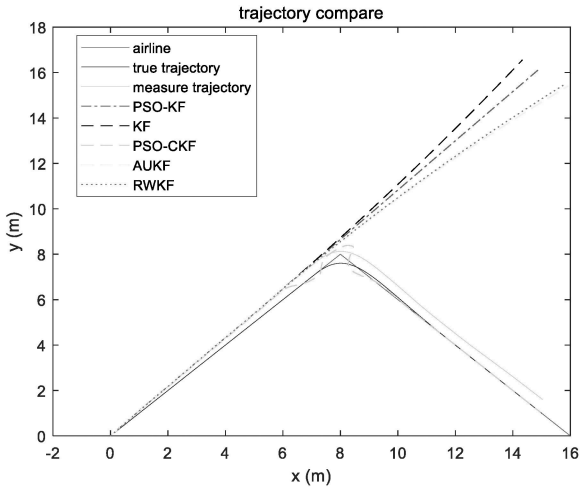

Figure 6. Trajectory comparison.

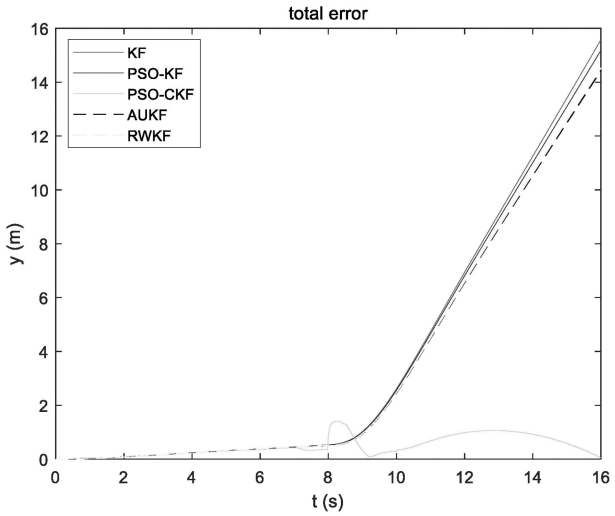

Figure 7. Comparison of prediction errors.

Table 1
Error Statistics of Different Forecast Durations

Filter Algorithm	1 s	5 s	9 s
KF	0.61	7.12	16.47
AUKF	0.50	6.54	14.40
RWKF	0.51	6.59	14.54
PSO-KF	0.53	6.79	15.16
PSO-CKF	0.60	0.57	0.95

accuracy of UAV position prediction. This improvement becomes more pronounced as the prediction duration increases.

The algorithm's tolerance to various noise conditions was examined through adjustments in noise type and magnitude. It was observed that the algorithm continued to perform effectively as the standard deviation of the UAV's acceleration random noise increased from 0.2 m/s^2 to 1 m/s^2. However, as constant noise reached 0.1 m/s^2, signs of degradation in algorithm performance became apparent. Subsequent research efforts will concentrate on optimising and enhancing the algorithm's performance in the presence of constant noise conditions.

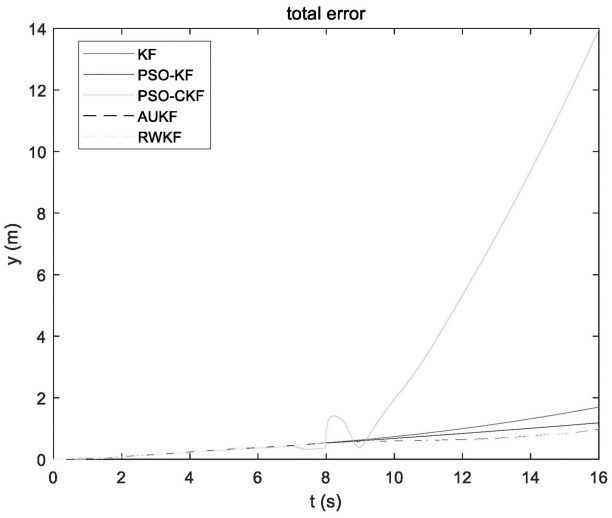

Figure 8. Starting the prediction after 7 s.

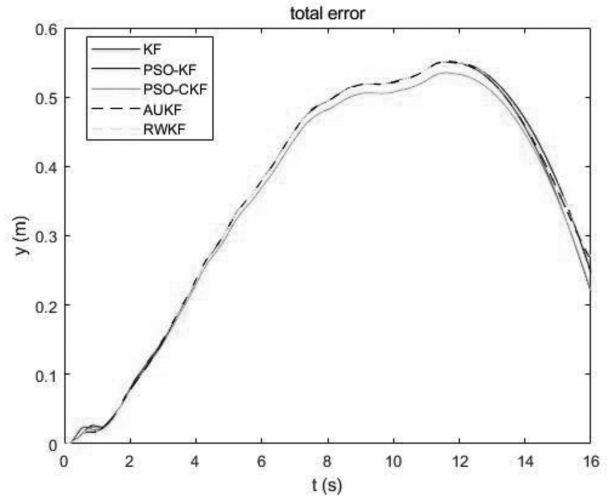

Figure 9. Starting the prediction after 12 s.

Simulations were also carried out for a specific scenario in which the UAV's flight path deviates from the pre-planned route due to external intrusion. The simulation results for this scenario are as follows:

From Fig. 8, it is evident that when prediction starts at the 7-second mark, the performance of the PSO-CKF is not as good as the KF. This is because the PSO-CKF provides incorrect prior information, leading to incorrect adjustments in the prediction results. However, when prediction starts at the 12-second mark, the PSO-CKF performs better than the KF. This is due to the real-time updates of noise covariance through the particle swarm algorithm and the presence of chi-squared tests, which help exclude incorrect prior information. Therefore, even if the UAV deviates from its pre-planned flight path due to intrusion, the enhanced method's predictions of the UAV's position will only experience short-term distortion.

6. Conclusion

This study focussed on the prediction of UAV positions and involved an in-depth investigation and improvement of the Kalman filtering algorithm. In terms of trajectory prediction, the PSO-CKF method outperformed other techniques, including KF, PSO-KF, and methods mentioned in [25] and [26], particularly when dealing with changes in path direction.

Through statistical analysis of the data presented in Table 1, it was observed that PSO-CKF significantly enhanced prediction accuracy, with improved performance as the prediction time horizon increased. Additionally, the study explored the algorithm's performance when the UAV deviated from its predefined flight path. The results indicated that even in cases where the UAV deviated from its intended course due to factors, such as intrusion, PSO-CKF exhibited distortion in UAV position prediction only in the short term.

Future research will concentrate on optimising and refining the algorithm to operate effectively in the presence of constant noise. In summary, this study has revealed the potential of PSO-CKF in enhancing UAV trajectory prediction accuracy and adapting to complex scenarios.

References

[1] L. Gupta, R. Jain, and G. Vaszkun, Survey of important issues in UAV communication networks, *IEEE Communications Surveys and Tutorials, 18*(2), 2016, 1123–1152.

[2] J. Zhao, Research on state information prediction of UAV under smart city, Ph.D. dissertation, Northern Polytechnic University, 2020.

[3] Z.M. Qi, Q.I. Huang, and H.L. Zhang, Intelligent unmanned cluster mission planning system architecture design, *Military Operations Research and Systems Engineering, 33*(3), 2019, 26–30.

[4] H.B. Duan, L. Xin. Y. Xu, G. Zhao, Eagle-vision-inspired visual measurement algorithm for UAV's autonomous landing, *International Journal of Robotics and Automation, 35*(2), 2020, 94–100.

[5] R. Dong, C. Liu, X. Wang, and X. Han 3D path planning of UAVs for transmission lines inspection, *International Journal of Robotics and Automation, 35*, 2020, 146–158.

[6] Y. Yan, Z. Lv, P. Huang, and J. Yuan, Rapid selecting UAVs for combat based on three-way multiple attribute decision, *International Journal of Robotics and Automation, 36,* 2021, 296–305.

[7] V. Doan, T. Thang, V. Than Dung, and S. Hirotaka, A cyborg insect reveals a function of a muscle in free flight, *Cyborg and Bionic Systems 2022,* 2022, 9780504.

[8] L. *Yu*, J. Zhao, Z. Ma, W. Wang, S. Yan, Y. Jin, and Y. Fang, Experimental verification on steering flight of honeybee by electrical stimulation, *Cyborg and Bionic Systems 2022,* 2022, 9895837.

[9] Z. Chen, Q. Liang, *Z.* Wei, X. *Chen*, Q. Shi, Z. Yu, and T. Sun, An overview of in vitro biological neural networks for robot intelligence, *Cyborg and Bionic Systems, 4*, 2023, 0001.

[10] C. Lidynia, R. Philipsen, and M. Ziefle, Droning on about drones—Acceptance of and perceived barriers to drones in civil usage contexts, *Proc. of the AHFE 2016 International Conference on Human Factors in Robots and Unmanned Systems*, , Florida, USA, 2017,317–329.

[11] M. Ayamga, S. Akaba, and A.A. Nyaaba, Multifaceted applicability of drones: A review, *Technological Forecasting and Social Change, 167*, 2021, 120677.

[12] X. He, Y. Su, and Y. Qiu, An improved unscented Kalman filter for maneuvering target tracking, *Journal of Physics: Conference Series, 2216*(1), 2022, 012010.

[13] A. Hafeez, M.A. Husain, S.P. Singh, and A. Chauhan, Implementation of drone technology for farm monitoring and pesticide spraying: A review. *Information Processing in Agriculture*, *10*(2), 2022, 192–203.

[14] M. Sibanda, O. Mutanga, V.G.P. Chimonyo, A.D. Clulow, C. Shoko, D. Mazvimavi, T. Dube, T. Mabhaudhi, Application of drone technologies in surface water resources monitoring and assessment: A systematic review of progress, challenges, and opportunities in the global south, *Drones, 5*(3), 2021, 84.

[15] S. Lee and Y. Choi, Reviews of unmanned aerial vehicle (drone) technology trends and its applications in the mining industry, *Geosystem Engineering, 19*(4), 2016, 197–204.

[16] M. Hammer, M. Hebel, M. Laurenzis, and M. Arens, Lidar-Based Detection and Tracking of Small UAVs, *Society of Photographic Instrumentation Engineers, Digital Library,* Berlin, Germany, 2018, 107990S-1–107990S-9.

[17] Z. Wu, J. Li, J. Zuo, and S. Li, Path planning of UAVs based on collision probability and Kalman filter, *IEEE Access, 6* 2018, 34237–34245.

[18] Y. Lin and S. Saripalli, Path planning using 3D Dubins curve for unmanned aerial vehicles, *International Conference on Unmanned Aircraft Systems (ICUAS),* Florida, USA, 2014, 296–304..

[19] S. Becker, R. Hug, W. Hübner, M. Arens, and B.T. Morris, Generating synthetic training data for deep learning-based UAV trajectory prediction, *arXiv:2107.00422,* 2021.

[20] B. Hu, H. Yang, L. Wang, and S. Chen, A trajectory prediction based intelligent handover control method in UAV cellular networks, *China Communications, 16*(1), 2019, 1–14.

[21] P. Shu, C. Chen, B. Chen, K. Su, S. Chen, H. Liu, F. Huang, Trajectory prediction of UAV based on LSTM, *Proc. 2nd International Conference on Big Data & Artificial Intelligence & Software Engineering (ICBASE),* Zhuhai, China, 2021, 448–451.

[22] R. Havangi, An adaptive particle filter based on PSO and fuzzy inference system for nonlinear state systems, *Automatika, 59*(1), 2018, 94–103.

[23] Q. Bai, Analysis of particle swarm optimization algorithm, *Computer and information science*, *3*(1), 2010, 180.

[24] N. Hassan and A. Saleem, Real time obstacle motion prediction using neural network based extended Kalman filter for robot path planning, *Kuwait Journal of Science, 50,* 2021, 1–20.

[25] F. Deng, H.-L. Yang, and L.-J. Wang, Adaptive unscented Kalman filter based estimation and filtering for dynamic positioning with model uncertainties, *International Journal of Control, Automation and Systems, 17*, 2019, 667–678.

[26] W. Wenhui, S. Gao, Y. Zhong, C. Gu, and A. Subic, Random weighting estimation for systematic error of observation model in dynamic vehicle navigation, *International Journal of Control, Automation and Systems, 14*,2016, 514–523.

Biographies

Jian Zhou received the Bachelor's degree in communication engineering from Chongqing University of Posts and Telecommunications in 2002, and the Master's degree in communication engineering from the University of Electronic Science and Technology of China in 2007. He is currently pursuing the Ph.D. degree with the University of Electronic Science and Technology of China. He currently serves as the Deputy Chief Designer with the China Mobile (Chengdu) Industrial Research Institute's 5G Networked Unmanned Aerial Vehicle Center. He is also a member of the NB-IoT Application Committee of Sichuan Province, China, and has been involved as a Key Contributor in the development of 6 IEEE standards and 2 national standards.

Yu Su received the Ph.D. degree in information and communication engineering from Northwestern Polytechnical University. He is currently a Senior Engineer and the Vice Dean with the China Mobile (Chengdu) Industrial Research Institute. In 2017, he received the National Technology Invention Award (Second Class) and is a recipient of the Special Government Allowance from the State Council of China.

Yuhe Qiu received the Bachelor's degree in communication engineering from Guilin Electronic Technology University in 2004, and the Master's degree in communication and electronics engineering from Tsinghua University in 2011. He is currently pursuing the Ph.D. degree with Southeast University. He currently serves as the Technical Director with the China Mobile (Chengdu) Industrial Research Institute's 5G Networked Unmanned Aerial Vehicle Center. His primary research areas include machine learning, communication technology, and 5G networked drone-related technologies.

Xiaoyou He received the Master's degree from Harbin Institute of Technology in 2014 and currently works as a Researcher with the China Mobile (Chengdu) Industrial Research Institute's 5G Networked Unmanned Aerial Vehicle Center. His main research focus is on drone navigation and control.

Zhihong Rao currently serves as the Ph.D. Supervisor with the University of Electronic Science and Technology of China and is the Chief Engineer of China Electronics Technology Group Corporation's China Electronics Technology Network Information Security Company Ltd.